



HAL
open science

POST SEISMIC DEFORMATION FOLLOWING THE APRIL 25,2015 GORKHA EARTHQUAKE: AFTERSLIP VERSUS VISCOUS RELAXATION.

François Jouanne, Ananta Prasad Gajurel, Jean-Louis Mugnier, Laurent Bollinger, Lok Bijaya Adhikari, Bharat Koirala, Nathalie Cotte, Roshanraj Bhattarai, Arnaud Pecher, Pascale Bascou, et al.

► To cite this version:

François Jouanne, Ananta Prasad Gajurel, Jean-Louis Mugnier, Laurent Bollinger, Lok Bijaya Adhikari, et al.. POST SEISMIC DEFORMATION FOLLOWING THE APRIL 25,2015 GORKHA EARTHQUAKE: AFTERSLIP VERSUS VISCOUS RELAXATION.. Journal of Asian Earth Sciences, 2019, 10.1016/j.jseaes.2019.02.009 . hal-02395962

HAL Id: hal-02395962

<https://hal.science/hal-02395962>

Submitted on 5 Oct 2022

HAL is a multi-disciplinary open access archive for the deposit and dissemination of scientific research documents, whether they are published or not. The documents may come from teaching and research institutions in France or abroad, or from public or private research centers.

L'archive ouverte pluridisciplinaire **HAL**, est destinée au dépôt et à la diffusion de documents scientifiques de niveau recherche, publiés ou non, émanant des établissements d'enseignement et de recherche français ou étrangers, des laboratoires publics ou privés.

1 POSTSEISMIC DEFORMATION FOLLOWING THE APRIL 25, 2015 GORKHA
2 EARTHQUAKE: AFTERSLIP VERSUS VISCOUS RELAXATION.

3
4 François Jouanne (1), Ananta Gajurel (2), Jean-Louis Mugnier (1), Laurent Bollinger (3), Lok
5 Bijaya Adhikari (4), Bharat Koirala (4), Nathalie Cotte (1), Roshanraj Bhattarai (2,1), Arnaud
6 Pecher (1), Pascale Bascou (1), Pascale Huyghe (1).

7
8 1 Univ. Grenoble Alpes, Univ. Savoie Mont Blanc, CNRS, IRD, IFSTTAR, ISTerre.

9 2 Department of Geology, Tribhuvan University, Ghantaghar, Kathmandu, Nepal

10 3 CEA, DAM, DIF, Arpajon, France.

11 4 Department of Mines and Geology, National Seismological Center, Kathmandu, Nepal.

12

13 Received in original form: 8 July 2017.

14

15 Abbreviated title suitable for page headings:

16 Postseismic deformation following the Gorkha earthquake.

17

18 Corresponding author:

19 François Jouanne,

20 Université de Savoie Mont Blanc, ISTerre,

21 F-73376 Le Bourget du Lac, France

22 Email : fjoua@univ-smb.fr

23 Tel : (33)608371432

24

25

26

27

28

29

30 SUMMARY.

31

32 . The postseismic deformation consecutive to the April 25, 2015 Gorkha earthquake (7.8
33 Mw) is estimated in this paper based on a cGNSS network installed prior to the earthquake and
34 supplemented by cGNSS stations installed after the main shock. Postseismic velocities are
35 obtained from recorded velocities corrected for interseismic deformation and seasonal
36 variations . The maximum postseismic displacement is found north of the rupture area, and
37 locally reached 100 mm between the earthquake and late 2016. The postseismic deformation
38 extends in the northern part of the rupture area whereas there is a lack of postseismic
39 deformation south of the rupture, along the southern part of the Main Himalayan Thrust. Three
40 hypotheses for the mechanisms controlling postseismic deformation are tested through
41 numerical simulations of the postseismic time series: viscous relaxation, afterslip or a
42 combination of these two mechanisms. We can exclude postseismic deformation controlled by
43 viscous relaxation of a thick deformation zone along the northern and lower flat of the MHT.
44 However, it is not possible to discriminate between postseismic deformation controlled by
45 either an afterslip along the MHT (northern part of the rupture zone, crustal ramp and lower flat
46 of the MHT) or a combination of afterslip along the MHT (northern part of the rupture zone,
47 crustal ramp) and viscous relaxation along a thin (~3km thick) low viscosity body centered on
48 the lower flat of the MHT.

49 **Keywords:**

50 Creep and deformation, Transient deformation, Asia, Seismic cycle, Space geodetic
51 surveys.

52

53

54

55 INTRODUCTION.

56 The April 25, 2015 Mw 7.8 Gorkha earthquake provides a unique opportunity to study
57 a large Himalayan earthquake with continuous GNSS data (Avouac et al., 2015), InSAR
58 investigations (e.g. Grandin et al., 2015) and good seismological data (Adhikari et al., 2015;
59 Baillard et al., 2017). The implementation of a cGNSS network, prior to the earthquake, has
60 also allowed to quantify the early postseismic surface deformation consecutive to this large
61 earthquake (Mencin et al., 2016).

62 The 2015 earthquake (Fig. 1) is a very good example to study the complexity of the seismic
63 cycle in a continental subduction zone: it indicates that the convergence along a main thrust is
64 consumed during various types of earthquakes (Mugnier et al., 2013), some of which partially
65 contributes to release the elastic strain of the Main Himalayan Thrust (Avouac et al., 2015).
66 This partial release has already been instrumentally measured in several oceanic subduction
67 environments; for example, in the Andean convergent margin, the main slip patch of the 2010
68 Mw 8.8 earthquake occurred in an area that was highly coupled and had already released slip
69 in 1960 (Melnick et al., 2012; Moreno et al., 2012). However, the 2015 Gorkha event provides
70 a unique opportunity to study the postseismic deformation: in an oceanic subduction zone,
71 GNSS data cannot be deployed in the marine area located above the rupture whereas 12 stations
72 were located all around the Gorkha rupture zone. Furthermore, during the weeks following the
73 main shock, the dataset has been completed by the deployment of other permanent or semi-
74 permanent GNSS stations (this paper).

75 Nonetheless, the mechanism controlling the postseismic deformation associated with the 2015
76 Gorkha event has not yet been studied in detail. Different mechanisms are usually inferred for
77 the postseismic deformation: afterslip or viscous relaxation. Given that the coseismic
78 displacement field for this earthquake has been estimated (e.g. Avouac, 2015) and the geometry
79 of the Main Himalayan Thrust is rather well imaged (Duputel et al., 2016), it is possible to
80 numerically simulate the GNSS time series illustrating the postseismic deformation in order to

81 determine the mechanisms controlling this deformation in Nepal. The Relax software (Barbot
82 et al., 2009) was used to model the postseismic deformation and three mechanisms have been
83 tested: afterslip, viscous relaxation or a combination of these two phenomena. We used a flap-
84 ramp-flat geometry (Elliott et al., 2016) with a southern and upper flat corresponding to the
85 geometry adopted by Grandin et al. (2016) to describe the coseismic slip distribution of the
86 Gorkha earthquake along this flat.

87

88 GEOLOGICAL SETTING.

89 The structure of the Himalaya results from the underthrusting of the Indian lithosphere
90 along the Main Himalayan Thrust (MHT) beneath the Tibetan Plateau (Argand, 1924). Great
91 earthquakes have episodically ruptured segments of the brittle upper part of the MHT (e.g.
92 Avouac et al., 2001; Mugnier et al., 2013). The Nepal earthquake of April 25, 2015 followed a
93 series of great earthquakes in Central Himalaya (Mugnier et al., 2011; Bollinger et al., 2014):
94 over the last two centuries, the city of Kathmandu was severely damaged in 1833, 1866, 1934.
95 The April 25, 2015 event (Fig. 1) is the first event that occurred along the MHT and which was
96 simultaneously recorded by numerous instruments: high-rate GPS (e.g. Avouac et al., 2015),
97 teleseismic waves (e.g. Fan and Shearer, 2015), SAR imaging (e.g. Lindsey et al., 2015), InSAR
98 and teleseismic waves (Grandin et al., 2016), strong-motion recordings (e.g. Bhattarai et al.,
99 2015) and a local seismometer network (Adhikari et al., 2015).

100 The rupture was mainly located to the NW of Kathmandu, at a depth of 13-15 km on a flat
101 portion of the Main Himalayan Thrust (MHT) that dips towards the N-NE by 7-10°. The
102 northern boundary of the main rupture corresponds to the transition towards a steeper crustal
103 ramp. This ramp, which is partly coupled during the interseismic period (Jouanne et al., 2017),
104 is only locally affected by the earthquake (Elliott et al., 2016). The southern boundary of the
105 rupture was near the leading edge of the Lesser Himalaya antiformal duplex (Mugnier et al.,

Commenté [p1]: Pas dans la biblio

Commenté [p2]: Pas dans la biblio

106 2017) and possibly near the frontal footwall ramp of the upper Nawakot duplex (Hubbard et al.,
107 2016). This rupture was affected by transversal structures: on the western side, a ~20° dipping
108 lateral ramp (Kumar et al., 2017), located beneath the Judi lineament (Mugnier et al., 2017) and
109 already defined by Kayal (2008), separates the main rupture zone from the nucleation area. On
110 the eastern side, a lateral ramp (Mugnier et al., 2017) located beneath the Gaurishankar
111 lineament (Kayal, 2008) separates the April 25, 2015 rupture from the May 12, 2015 (Mw 7.2)
112 rupture.

113

114 DATA ACQUISITION AND ANALYSIS.

115

116 After the April 25 Gorkha earthquake, we installed a GNSS network designed to record
117 postseismic deformation induced by this Mw 7.8 earthquake. We installed five permanent
118 GNSS stations in June 2015 and 11 episodic GNSS stations between June and December 2015.
119 Seven of these stations were measured again in November 2016 (Figs. 2 and 3). We analyzed
120 these data together with the continuous GNSS networks established by LDG-DASE, Caltech
121 (www.unavco.org), Central Washington University (<http://www.geodesy.cwu.edu>) and with
122 data from the GNSS sites defined in the ITRF2014 reference frame (ARTU,
123 BADG,BAKU,BJFS, BJNM, CHUM, CUSV, GUAO, HYDE, IISC, IRKJ, IRKM, KIT3,
124 KUWT, LHAZ, MDVJ, POL2, SGO, SHAO, TALA, TASH, TCMS, TEHN, TNML, URUM,
125 ZECK).

126 The data were analyzed using the Bernese 5.2 software, with absolute antenna phase center
127 offset models, together with precise orbits, earth rotation parameters, ocean tidal loading and
128 atmospheric tidal loading estimates. Velocities and time series were estimated in the ITRF2014
129 reference frame (Altamimi et al., 2016) with discontinuities associated with this reference frame
130 and expressed in terms of the India fixed reference frame by the use of the rotation pole

Commenté [j13]: Je comprend pas à quoi correspondent ces données, d'où elles proviennent !

Commenté [j14]: ETRANGE : EST-CE UTILE ? RETIRER OU METTRE UNE REFERENCE ?

131 proposed by Ader et al. (2012). This rotation pole, originally proposed to describe the motion
132 of India relative to ITRF2005, rather describes accurately the India plate motion in the
133 ITRF2014 reference frame, as shown by Jouanne et al. (2017) and as exemplified by the lack
134 of velocity of the cGPS SIM4 station located on the India plate (Fig. 3). In any case, the
135 eventual velocities changes introduced by the **change of ITRF** are negligible compared to the
136 large postseismic displacements.

Commenté [j15]: Changement entre quoi ? et introduit par qui ?

137 We followed the resolution strategy with (1) an initial ionosphere-free analysis with calculation
138 of the residuals; (2) a residual analysis; (3) code-based wide-lane ambiguity resolution for all
139 baselines (Melbourne, 1985; Wübbena, 1985), using differential code bias (DCB) files when
140 available and calculation of the ionosphere-free solution with the introduction of resolved
141 Melbourne-Wübbena linear combination ambiguities; (4) phase-based wide-lane (L5)
142 ambiguity resolution for baselines < 200 km and computation of the ionosphere-free solution
143 with the introduction of resolved ambiguities; (5) resolution of the previously unresolved
144 ambiguities for baselines < 2000 km using the quasi ionosphere-free strategy of resolution; (6)
145 direct L1/L2 ambiguity resolution for baselines < 20 km with the introduction of an ionosphere
146 model; (7) calculation of the normal equations; (8) a compatibility test between the daily free
147 solution and ITRF2014 solution, selection of compatible ITRF2014 stations and (9)
148 transformation of the daily normal equation in the ITRF2014 reference frame with a six-
149 parameter Helmert solution (three translation parameters and three rotation parameters) using
150 the ITRF2014 selected stations. During these steps, site-specific troposphere parameters were
151 estimated every two hours.

152 Normal equations were analyzed **together** to determine accurate velocities in the ITRF2014
153 reference frame with the introduction of ITRF2014 coordinates and velocities. Outliers and new
154 discontinuities were detected using the “Find Outliers and Discontinuities in Time Series” tool
155 in the Bernese 5.2 software that takes annual seasonal fluctuations into account and reduces,

Commenté [j16]: Plutôt : « simultaneously ?

156 step by step, the discrepancy between the functional model and the time series due to statistical
157 adjustment (Ostini et al., 2008). As the Bernese 5.2 software underestimates the daily errors
158 given that systematic errors or mismodeled parameters are not included in the formal error
159 (Hugentobler et al., 2001), we rescaled the formal errors by multiplying them by a factor of 10
160 to obtain a more realistic estimated error.

161

162 RESULTS: POSTSEISMIC DISPLACEMENTS AT THE SURFACE.

163

164 We consider that displacements contain three superimposed signals: the interseismic
165 displacements, the postseismic displacements and the seasonal signal associated with the
166 loading of the Ganga Plain during the monsoon and its unloading during the dry season
167 (Bettinelli et al., 2008; Fu and Freymueller, 2012; Gualandi et al., 2016). In order to analyze
168 postseismic displacements, we removed the interseismic displacements that were either
169 measured before the Gorkha earthquake for the sites that already existed before this event
170 (BESI, BRN2, CHLM, DAMA, GUMB, KKN4, KLDN, LMJG, NAST, ODRE, RMJT, RMTE,
171 SNDL, SYBC, TPLJ) (Jouanne et al., 2017) or were estimated using interseismic deformation
172 modellings performed by Jouanne et al. (2017) for the new GNSS sites (Fig. 2).

173 In order to evaluate the seasonal annual components, we analysed the time series
174 between 2000 and April 2015 for the available cGNSS stations (BESI, BRN2, CHLM, DAMA,
175 GUMB, KKN4, KLDN, LMJG, NAST, ODRE, RMJT, RMTE, SNDL, SYBC, TPLJ) using
176 the FODITS program in the Bernese 5.2 software (Ostini et al. 2008). For the cGNSS stations
177 installed after the earthquake, we interpolated in space the values obtained from the cGNSS
178 stations that had been installed for several years to correct the time series for the components
179 of the seasonal signal (annual signal amplitudes and phase difference, Table 1).

180

Commenté [j17]: Le critère de choix ou de disponibilité n'est pas clair.

181 The postseismic displacements for the period when most of the GNSS stations were
182 available (between June 24, 2015 and late 2016) is shown (Fig. 3) to compare site displacement
183 measured during the same time span. Postseismic displacements are characterized by the
184 southward displacements of the points north of the Gorkha rupture (CHLM, GUMB, TSM1).
185 The station that recorded the greatest postseismic displacement is CHLM (Fig. 3) located to the
186 north of the rupture, with 40 mm of southward displacement between April 25 and June 24 and
187 100 mm of southward displacement between June 24, 2014 and late 2016. The points located
188 in the northern part of the rupture zone (KKN4, GURJ, BALA) are affected by moderate
189 southward postseismic displacements, whereas the points located at the southern end of the
190 rupture, near to and south of Kathmandu (CHIR, DAMA, NAST and XYAK), are affected by a
191 negligible postseismic displacement. It should be noted that the points at the western part of the
192 rupture (LMJG, GORK and ANBU) are not affected by postseismic displacements whereas the
193 points located several kilometers to the east of the April 25, 2015 rupture (CHAR, JIR2,
194 MALU) are affected by significant postseismic displacements reaching 35 mm (Fig. 3). Given
195 that these points were installed after the May 12, 2015 Mw 7.2 main aftershock, these
196 postseismic displacements may be related to the postseismic deformation induced by this
197 earthquake.

198 Significant postseismic displacements are therefore restricted to the northern part of the rupture
199 zone and to an area to the north of it (Figs. 3 and 4). It is important to note that there are no
200 clear postseismic displacements to the south of the Gorkha earthquake rupture and, like Mencin
201 et al. (2016), we exclude the occurrence of a significant afterslip along the southern part of the
202 MHT. Therefore, the slip deficit along the MHT south of Kathmandu is not resorbed
203 aseismically by a slip along the MHT from the rupture zone to the MFT where the MHT
204 emerges. The slip deficit could then possibly be resorbed by a future large earthquake between
205 the southern end of the rupture near Kathmandu, and the MFT near the Ganga Plain, as has

206 probably already happened in the 1866 earthquake (Oldham, 1883; Szeliga et al., 2010), or by
207 a larger earthquake rupturing the locked fault zone from the brittle-ductile transition zone to the
208 surface, in a similar way as in the subduction zones (Melnick et al., 2012; Moreno et al., 2012)
209 or to the 1934 Nepal-Bihar earthquake (e.g. Mugnier et al., 2013).

210 As postseismic deformation is primarily characterized by southward displacements, we
211 illustrate in Figure 4 the postseismic deformation with the time series for the south component
212 corrected for the interseismic component and the seasonal signal in the India fixed reference
213 frame. The time series present a progressive decrease in postseismic displacement with time,
214 which suggests a progressive dissipation of the stress perturbation induced by the earthquake.
215 The CHLM time series presents a jump corresponding to the May 12 Mw 7.2 main aftershocks,
216 whereas the other stations were not significantly affected or were installed too late to record
217 this coseismic displacement. The GUMB and DCN4 station time series present anomalous
218 displacements respectively 340 to 480 days and 420 to 640 days after the main shock.
219 Moreover, the anomaly affecting the GUMB time series, which began respectively in April
220 2016, cannot be explained by the monsoon that began two months later, whereas the anomaly
221 affecting the DCN4 time series, which began in June 2016 is close to the beginning of the
222 monsoon. We assume that these local variations are induced by local phenomena such as local
223 unstabilities induced by the main shock.

224

225 MODELING POSTSEISMIC- DISPLACEMENT.

226 We have chosen to test the origin of the progressive release using three hypothesis with
227 the Relax 1_0_7 software (Barbot et al., 2009; Barbot and Fialko 2010; Bruhat et al., 2011;
228 Rousset et al., 2012): a postseismic deformation controlled by afterslip, viscous relaxation of
229 the stress perturbation and an association of these two mechanisms.

230 This software computes the displacement and stress due to dislocations and the nonlinear
231 postseismic time-dependent deformation, the latter either controlled by viscous bodies with

232 power-law rheology or by rate-strengthening friction faults. This software takes into account
233 gravity and is based on a Fourier-domain elastic Green's function and an equivalent body-force
234 representation of deformation mechanisms. Ce software est appliqué sur un maillage régulier,
235 et dans le cas du séisme de Gorkha, nous avons utilisé une zone d'étude de 50 km de large sur
236 70 km de large avec une maille élémentaire de 3 km.

237 For these modellings, we use the same MHT geometry as the one used for the pre-
238 earthquake deformation (Jouanne et al., 2017) (Fig. 5); this geometry also fits with the location
239 of the rupture zone proposed by Grandin et al. (2016) and in Figure 6. The geometry of the
240 MHT is formed by a succession of flats and ramps characterized by a southern large flat (95-
241 100 km) dipping 7° northward, a crustal ramp dipping 27° northward between 15 and 25 km
242 and a northern flat dipping 7° northward as illustrated by receiver-function data (Duputel et al.
243 2016).

244 As postseismic displacements only affected stations north of Kathmandu, postseismic
245 slip along the MHT did not affect all the upper flat of the MHT but only its northern parts. If
246 we consider the points BALE, KKN4 and GURJ (Fig. 3 and 4) that are nearly at the same
247 distance from the upper flat-ramp connection, it appears that the eastern one (BALE) is affected
248 by a more important postseismic displacements than the two others located in the western part
249 of the upper flat of the MHT. We have then considered that these surficial variations of the
250 displacement reflect the afterslip distribution along the MHT. We have considered in our
251 simulation a segment of the upper flat affected by an afterslip wider in the eastern part of the
252 upper flat than in the western part (Fig. 9). Spatial variations in the time series have led us to
253 consider a 25 km wide western segment and a 40 km wide eastern segment and the boundary
254 between these two segments coincides with the western edge of the Mai 12, 2015 rupture and
255 with the Gaurishankar lateral ramp as illustrated in Figure 1. This spatial variation also reflects
256 interseismic coupling variations between the western and eastern parts: the western part was
257 completely locked whereas the eastern part was only partially locked with a coupling of 0.7
258 (Fig. 8) (Jouanne et al., 2017).

259

260 To test the models, we used a time series that was corrected from interseismic velocities
261 and seasonal components. For the GUMB and DCN4 time series, which present an unexpected
262 behavior, we suspect local superficial effects superimposed on postseismic signal; we have
263 therefore chosen to exclude these data from the modeling.

264 The preferred solutions were selected using the comparison between the observed and simulated
265 time series (Fig. 7) with the estimation of WRMS for each simulation.

266

267 *Viscous relaxation model.*

268 The estimation of the coupling during the interseismic period (Betinelli et al., 2006;
269 Ader et al., 2012; Jouanne et al., 2017) suggests a ductile behavior along the northern flat of the
270 MHT. We therefore test the hypothesis that postseismic displacements reveal a viscous
271 relaxation of the stress perturbation induced by the main shock and its main aftershocks. The
272 ductile behavior is temperature dependant (Scholz, 1998) and does not occur in the brittle crust.
273 Viscous relaxation is therefore excluded for the upper flat and the ramp characterized by a
274 temperature lower than 375°C (Robert et al., 2011). Hereafter, we assume that the lower flat
275 only accommodates viscous relaxation.

276 In this simulation, a low viscous body corresponding to the deeper part of the Main Himalayan
277 Thrust is embedded in an elastic half space (Fig. 5a). The parameters to be determined are the
278 viscosity and the thickness of this body. We have chosen to explore the following ranges of
279 values: viscosity of the body from 10^{17} to 10^{19} Pas. and thickness of the body from 0 to 12 km.

280 The WRMS is always greater than 17 mm and no solution is clearly favored amongst the 200??
281 numerical runs performed to determine the parameter influence and summarized on Figure 7a.

282

283 *Afterslip model.*

Commenté [j18]: Une reference pour justifier ce choix !

284 If the postseismic displacements are controlled by an afterslip induced by the April 25
285 2015 Mw 7.9 earthquake, these displacements can be simulated by a progressive release of the
286 stress perturbation due to the main shock. We assume that the afterslip takes place (Fig. 5) along
287 the northern part of the upper flat of the MHT affected by the April 25, 2015 earthquake, along
288 the crustal ramp north of the rupture zone and along the lower flat north of this ramp.
289 We assign rate-strengthening properties derived from laboratory experiments (Dieterich, 1979;
290 Ruina,1983) to these three fault segments with:

$$V = 2 \dot{\gamma}_0 \sinh \frac{\Delta\tau}{(a - b)\sigma} \quad (\text{eq. 1})$$

291
292 Where V is the slip on the fault, $\Delta\tau$ is the stress perturbation induced by the earthquake that is
293 progressively released by the afterslip, $\dot{\gamma}_0$ and $(a - b)$ are constitutive parameters and σ the
294 stress drop during the earthquake.

295 The initial stress perturbation associated to the coseismic slip distributions of the April 25, 2015
296 and May 12, 2015 earthquake estimated by Grandin et al. (2016) (Fig. 6) is calculated with the
297 Relax1_0_7 software.

298 We explore the parameters space (Fig. 7b) formed by $\dot{\gamma}_0$ (from 50 to 800 mm/year), and the
299 friction along the considered planes (from 0 to 1.2) for an $(a - b) \sigma$ values of 45 MPa. Amongst
300 the 5000000?? numerical runs performed to determine the parameter influence (Figure 7b), a
301 minimum of 3.9 mm is found for the WRMS (Fig. 7b) linked to friction coefficient and $\dot{\gamma}_0$ of
302 0.9 and 480, respectively.

303
304 *Afterslip and viscous relaxation model.*

305 This simulation takes into account the hypothesis that the northern flat may be a zone affected
306 by ductile deformation (e.g. Elliott et al., 2016 VERIFIER) channel (Beaumont et al., 2001),

Commenté [j19]: VERIFIE :je ne suis pas sur vérifie.....

Commenté [j110]: Quel type de logiciel a utilisé Grandin ?
Je suis surpris qu'il n'y ai pas de références concernant le stress drop et la contrainte de Coulomb ?

Commenté [j111]: Une reference pour justifier ces plages de valeur ?

331 between the two hypotheses -afterslip alone or afterslip combined with viscous relaxation on
332 the lower flat.

333 All the retained simulations indicate (Figures 6c): a) a moderate afterslip along a large part of
334 the ramp, b) a significant afterslip along the northern part of the upper flat; c) large afterslip
335 where the coseismic slip gradient was high: at the upper flat/crustal ramp transition, locally in
336 the rupture area and near the southern boundary of the rupture; d) the lack of significant
337 postseismic displacements near most of the southern border of the numerical model on the upper
338 flat segment of the MHT affected by afterslip. Afterslip along the southern part of the upper
339 flat, to the south of the southern border of the numerical model is therefore excluded, as we had
340 *a priori* assumed for the determination of the mesh based on the nearly null postseismic
341 displacement measured south of the Gorkha rupture zone. The models nonetheless indicate a
342 high post seismic displacement at the western edge of the mesh and suggest that post-seismic
343 motion could extend farther west of this zone.

344

345 *Evolution of the afterslip along the MHT.*

346 The slip velocity evolution through over time and space of our preferred model indicates that
347 (Fig. 9): the lower flat of the MHT is affected by a slow large-scale afterslip decreasing over
348 time, whereas the crustal ramp is affected by a negligible afterslip without significant lateral
349 variations. The northern part of the upper flat is characterized by local patches of high velocity
350 afterslip; the latter reached 2 m/year with a significant lateral variability and a significant
351 decrease between $D + 40$ days and $D + 180$ days. The areas of the upper flat affected by
352 significant slip velocity are located close to the flat-ramp transition that corresponds to the
353 northern boundary of the rupture. Areas of the upper flat locally affected by a significant slip
354 velocity are characterized by local high coseismic displacement gradient in Grandin et al.'s
355 model (2016) and then to local high deviatoric stress to be release. Locally, slip also occurred

356 southward in areas near the southern end of the mesh, upper flat segment of the MHT affected
357 by afterslip.

358 Our modelling suggests changes of width of the upper flat of the MHT affected by afterslip
359 (Fig. 8). These spatial changes and the significant misfits between observed and simulated time
360 series mainly observed for the JIR2 and GURJ stations may reflect spatial friction coefficient
361 variations not modelled by our simple models.

362

363 *The afterslip properties along the MHT.*

364 In the Relax software, it is possible to only consider one single afterslip property
365 (friction ratio and constitutive parameters) for all of the fault segments. As a result, we have
366 then considered the same properties for the upper flat, crustal ramp and lower flat of the MHT.
367 Our preferred model that allows a good fit with the observed time series (Fig. 7b?) has been
368 obtained with $\dot{\gamma}_0 = 450$ mm/year and a friction of 0.9 for (a-b) $\sigma = 45$ Mpa. The best-fit models
369 consider two distinct parts for the upper flat of the MHT.

370 DISCUTER CES VALEURS PAR RAPPORT A CE QUI EXISTE DANS LA
371 LITTERATURE ET PAR RAPPORT A DE QUE CES GRANDEURS REPRESENTENT
372 (ELLES N'ONT PAS UNE VALEUR UNIQUEMENT DANS CE MODELE, ENFIN J
373 ESPERE)

374 (a-b) σ ?

375 A friction coefficient of 0.9 would mean a friction angle close to 41° and is very high in
376 respect to the usually inferred values. For example the friction angle was estimated at 20° for
377 the Indian crust in the modeling of Berger et al. (2003). Values greater than 41° were
378 nonetheless found experimentally for numerous rocks (Kulhawi, 1975).

379 The interseismic and postseismic modelings therefore suggest a frictional variation
380 along the upper MHT on both sides of the Gaurishankar lateral ramp.

Commenté [M12]: Cette partie est largement une reprise du paragraphe précédent, il faudrait peut-être regrouper

Commenté [j113]: JE SUIS PAS SUR QUE CA SOIT JUSTE VU QUE TU IMPOSES TA LIMITE AVANT LA MODELISATION ; !

Commenté [j114]: JE COMPREND PAS CE QUE TU VEUX DIRE

Commenté [j115]: COMME TU N'INTROUIT PAS LA RUPTURE DE MAI A L'EST, TU N'AS PAS DE PERTURBATION DES CONTRAINTES A L'EST ET DONC PAS DE POST A L'EST ! PEUT ETRE NE PAS EN PARLER

381

382 *Viscous relaxation controlled by a low viscosity zone along the lower flat of the MHT.*

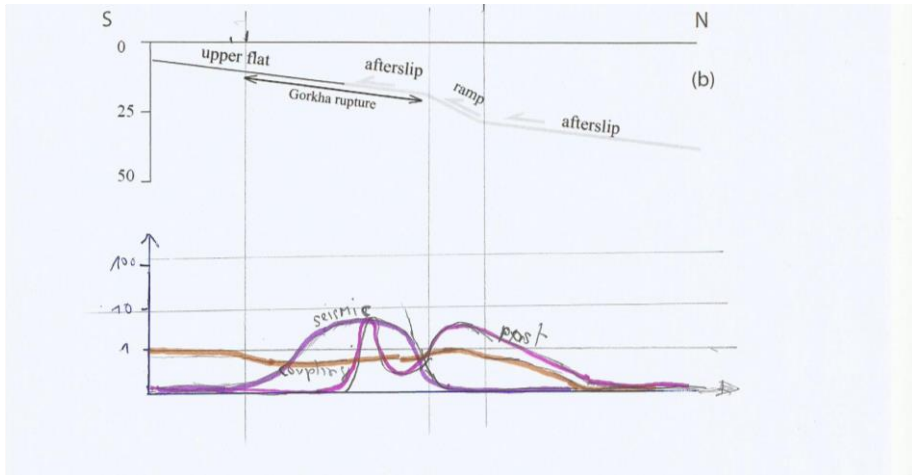
383 The time series for the stations located above the rupture zone, or to the south of it, are not
384 correctly simulated by a viscous relaxation controlled by a ductile body centered on the northern
385 flat. In the numerical models where afterslip along the upper parts of the MHT has been
386 introduced, the low viscosity body has to be thin (close to 3 km) to minimize the discard
387 between model and data and in this case the discard is small.

388 We therefore believe that viscous relaxation controlled by a low viscosity body cannot alone
389 explain the recorded postseismic deformation and another source of deformation located to the
390 south of the deep flat (i.e. afterslip) is needed.

391 Nonetheless, the low viscosity body is a reasonable assumption as it may control the
392 low coupling along the lower flat documented for the interseismic period (Fig. 8). Furthermore,
393 low viscosity level has been suggested from the interpretation of deep image of the Himalayan
394 crust (e.g. Zhao et al., 1993; Nelson et al., 1996).

395 A channel flow model (Beaumont et al., 2001) was even proposed to describe the Himalayan
396 tectonics evolution and is based on a very thick ductile zone (more than 10 km
397 thick), so thick that the horizontal velocity depicts a peculiar gradient, with a
398 maximum velocity in the center of the ductile zone. Our results nonetheless suggest that the
399 ductile zone is less than 3(or 5?) km thick beneath the very southern part of the Tibet plateau.

400 Therefore, we suggest that the recent tectonics of Himalaya is not controlled by a channel flow
401 deformation at depth, although our results does not preclude a thicker ductile zone towards the
402 north.



Commenté [M16]: CETTE FIGURE ME PARAIT INDISPENSABLE POUR SYNTHETISER DE MANIERE ATTRACTIVE TOUT CE TRAVAIL.....

403
 404 *Fig. 10 Comparison between interseismic coupling ratio, seismic slip and afterslip coupling*
 405 *ratio (pour illustrer le paragraphe ci-dessous!). Les valeurs pourraient être prises sur une seule*
 406 *coupe ou correspondre à une moyenne d'un segment de largeur de la rupture, ceci projeté*
 407 *perpendiculairement à la rampe,*

408
 409 **Summary**

410 We then interpret our results as (1) a large-scale afterslip or a viscous relaxation of a thin zone
 411 (~3 km thick) of high fluidity along the lower flat of the MHT and (2) a moderate afterslip along
 412 the crustal ramp that prolongates down-dip the Gorkha rupture as well as (3) a high-velocity
 413 small-scale afterslip along the southern boundary of the segment and (4) a high-velocity
 414 afterslip in areas characterized by a significant coseismic slip gradient during the earthquake.
 415 This pattern where a moderate afterslip along the crustal ramp prolongates down-dip the rupture
 416 till the ductile levels as also been shown for the postseismic deformation following the 2005
 417 Balakot-Bagh earthquake (Jouanne et al., 2011; Wang and Fialko, 2014), for the deformation
 418 consecutive to the 1995 Chi-Chi earthquake (Yu et al., 2003; Perfettini and Avouac, 2004) and
 419 for the 1995 Jalisco earthquake (Hutton et al., 2001).

Commenté [M17]: Moi je représenterai bien sur un même diagramme, en dessous de la coupe les mouvements co, post et inter sismique, ce qui permettra de discuter de la signification du couplage inter-sismique ! Tu montreras en particulier que toute la zone de rupture n'était pas complètement bloquée

Commenté [j18]: je comprend pas vraiment le sens de large-scale

Commenté [M19]: Dans ces deux cas on peut estimer un déplacement des compartiments de par et d'autre du MHT ? il faudrait donner des valeurs

420

421 CONCLUSION.

422 The postseismic velocity field clearly shows a lack of displacements to the south of
423 Kathmandu. An afterslip along the southern part of the rupture area of the Gorkha earthquake
424 and along the southern segment of the MHT unaffected by the main shock is then clearly
425 excluded. The slip deficit along the southern part of the upper flat of the MHT, between
426 Kathmandu and the Ganga Plain, would be probably transferred along the MHT by an
427 earthquake of large magnitude, as was possibly the case after the previous 1833 large
428 earthquake along this segment of the MHT: the 1833 earthquake was followed by a second
429 shock in 1866, in the vicinity of Kathmandu, possibly to the south. To the west and east of the
430 Gorkha rupture, postseismic displacements are nearly negligible, and afterslip does not affect
431 the upper flat areas of the MHT to the west of the rupture zone.

432 The simulation of the time series using the Relax software suggest that the postseismic
433 deformation consecutive to the April 25, 2015 earthquake is controlled by an afterslip along the
434 northern part of the upper flat of the MHT, corresponding to the northern part of the rupture, an
435 afterslip along the crustal ramp and an afterslip or viscous relaxation of thin (~3 km thick)
436 ductile zone along the lower flat of the MHT of Il manque des estimations numériques 200 ? mm
437 dans l'année suivante en moyenne ?. Viscous relaxation along a ductile body centered on the
438 lower flat of the MHT alone cannot explain the postseismic deformation.

439

440 ACKNOWLEDGMENTS.

441 The figures and map were prepared using the Generic Mapping Tools software (Wessel
442 and Smith, 1995) and Paraview software (Ahrens et al., 2005; Ayachit, 2015). This material is
443 partially based on data provided by the Nepal permanent GNSS network (DMG, Caltech,
444 DASE) and data services provided by the UNAVCO Facility with support from the National

Commenté [M20]: Pas si négligeable que ça sur le maillage (coin inférieur gauche !)

Commenté [M21]: Mon problème dans ce papier, c'est que tu regarde un segment du plat supérieur qui comprend aussi le séisme de mai à l'ouest, mais on sait pas si tu en tiens compte dans la modélisation pour le chargement.

Commenté [M22]: Il manque des estimations numériques 100 mm dans l'année suivante en moyenne ?

Commenté [M23]: Il manque des estimations numériques 100 mm dans l'année suivante en moyenne ?

Commenté [M24]:

Commenté [p25]: Pas dans la biblio

Commenté [p26]: Pas dans la biblio

445 Science Foundation (NSF) and National Aeronautics and Space Administration (NASA) under
446 NSF Cooperative Agreement No. EAR-0735156. Funds have been provided by the Labex
447 OSUG@2020, by INSU-CNRS, by the AAP of Savoie Mont Blanc University by the IRD and
448 by the ANR Bhoutanepal.

Commenté [p27]: ,

449

450 REFERENCES

451

452 Ader, T., Avouac, J.P., Liu-Zeng, J., Lyon-Caen, H., Bollinger, L., Galetzka, J., Genrich, J.,
453 Thomas, M., Chanard, K., Sapkota, S., Rajaure, S., Shrestha, P., Ding, L., Flouzat, M., 2012.
454 Convergence rate across the Nepal Himalaya and interseismic coupling on the Main Himalayan
455 Thrust: implications. *J. Geophys. Res.* 117, B04403. <http://dx.doi.org/10.1029/2011JB009071>.

456

457 Adhikari, L.B., Gautam, U.P., Bhattarai, M., Kandel, T., Gupta, R.M., Timsina, C., Maharjan,
458 N., Maharjan K., Dahal, T., Hoste-Colomer, R., Cano, Y., Dandine, M., Guilhem, A., Merrer,
459 S., Roudil, P., Bollinger, L., 2015. The aftershock sequence of the April 25 2015 Gorkha-Nepal
460 earthquake. *Geophys. J. Int.* 203, 2119–2124.

461

462 Altamimi, Z., Rebischung, P., Métivier, L. and Xavier, C., 2016. ITRF2014: A new release of
463 the International Terrestrial Reference Frame modeling nonlinear station motions, *J. Geophys.*
464 *Res. Solid Earth*, 121, doi:10.1002/2016JB013098.

465

466 Argand, 1924. La tectonique de l'Asie. 104 p. Compte rendu du congrès géologique
467 international (1922). Vaillant-Carmane press (Liege, Belgium).

468

469 Avouac, J.P., Bollinger, L., Lavé, J., Cattin, R., Flouzat, M., 2001. Le cycle sismique en
470 Himalaya, *Comptes Rendus de l'Academie de Sciences - Serie IIa: Sciences de la Terre et des*
471 *Planètes*. doi:10.1016/S1251-8050(01)01573-7

472

473 Avouac, J.-P., Meng, L., Wei, S., Wang, T., Ampuero, J.P., 2015. Lower edge of locked Main
474 Himalayan Thrust unzipped by the 2015 Gorkha earthquake. *Nature Geoscience*, ISSN 1752-
475 0894.

476

477 Baillard, C., Lyon-Caen, H., Bollinger, L., Rietbrock, A., Letort, J., & Adhikari, L. B., 2017.
478 Automatic analysis of the Gorkha earthquake aftershock sequence: evidences of structurally
479 segmented seismicity. *Geophysical Journal International*, 209(2), 1111-1125.

480

481 Barbot, S., Fialko, Y., 2010. Fourier-domain Green's function for an elastic semi-infinite solid
482 under gravity, with applications to earthquake and volcano deformation, *Geophys. J. Int.*,
483 182(2), 568–582, doi:10.1111/j.1365- 246X.2010.04655.x.

484

485 Barbot, S., Hamiel, Y., Fialko, Y., 2008. Space geodetic investigation of the coseismic and
486 postseismic deformation due to the 2003 Mw 7.2 Altai earthquake: Implications for the local
487 lithospheric rheology, *J. Geophys. Res.*, 113(B03403), doi:10.1029/2007JB005063.

488

489 Barbot, S., Fialko, Y., Bock, Y., 2009. Postseismic Deformation due to the Mw 6.0 2004
490 Parkfield Earthquake: Stress-Driven Creep on a Fault with Spatially Variable Rate-and-State
491 Friction Parameters, *J. Geophys. Res.*, 114(B07405), doi:10.1029/2008JB005748.

492

493 Barbot, S., Fialko Y., 2010. A unified continuum representation of postseismic relaxation
494 mechanisms: semianalytic models of afterslip, poroelastic rebound and viscoelastic flow, -
495 *Geophys. J. Int.*, 182(3), 1124–1140, doi:10.1111/j.1365-246X.2010.04678.x.

496

497 Beaumont, C., Jamieson, R.A., Nguyen, M.H., Lee, B., 2001. Himalayan tectonics explained
498 by extrusion of a low-viscosity crustal channel coupled to focused surface denudation. *Nature*
499 414, 738–742.

500

501 Bettinelli, P., Avouac, J.P., Flouzat, M., Jouanne, F., Bollinger, L., Willis, P., Chitrakar, G.R.,
502 2006. Plate motion of India and interseismic strain in the Nepal Himalaya from GPS and DORIS
503 measurements. *J. Geod.* <http://dx.doi.org/10.1007/s00190-006-0030-3>.

504

505 Bettinelli, P., Avouac, J.-P., Flouzat, M., Bollinger, L., Ramillien, G., Rajaure, S., Sapkota, S.,
506 2008. Seasonal variations of seismicity and geodetic strain in the Himalaya induced by surface
507 hydrology. *Earth Planet. Sci. Lett.* 266, 332–344.

508

Commenté [p28]: Absent du texte

Commenté [p29]: Absent du texte

509 Berger, A., Jouanne, F., Hassani, R., Mugnier, J.L., 2004. Modelling the spatial distribution of
510 present-day deformation in Nepal: how cylindrical is the Main Himalayan Thrust in Nepal?
511 *Geophys. J. Int.*, 156, 94–114.

512

513 Bhattarai, M., Adhikari, L. B., Gautam, U. P., Laurendeau, A., Labonne, C., Hoste-Colomer,
514 R. & Hernandez, B., 2015. Overview of the large 25 April 2015 Gorkha, Nepal, earthquake from
515 accelerometric perspectives. *Seismological Research Letters*, 86(6), 1540-1548.

516

517 Bilham, R., Larson, K., Freymueller, J. Idylhim members (Jouanne, F., Le Fort, P., Leturmy, P.,
518 Mugnier, J.L., Gamond, J.F., Glot, J.P., Martinod, J., Chaudury, N.L., Chitrakar, G.R., Gautam,
519 U.P., Koirala, B.P., Pandey, M.R., Ranabhat, R., Sapkota, S.N., Shrestha, P.L., Thakury, M.C.,
520 Timilsina, U.R., Tiwari, U.R., Vidal, G., Vigny, C., Galy, A., De Voogd, B.), 1997. GPS
521 measurements of present-day convergence across the Nepal Himalaya. *Nature* 386, 1–94.

522

523 Bollinger, L., Sapkota, S. N., Tapponnier, P., Klinger, Y., Rizza, M., Van der Woerd, J.,
524 Tiwari, D. R., Pandey, R., Bitri, A., Bes de Berc S., 2014. Estimating the return times of great
525 Himalayan earthquakes in eastern Nepal: Evidence from the Patu and Bardibas strands of the
526 Main Frontal Thrust, *J. Geophys. Res. Solid Earth*, 119, doi:10.1002/2014JB010970.

527

528 Bruhat L, Barbot S, Avouac JP, 2011. Evidence for postseismic deformation of the lower crust
529 following the 2004 Mw6. 0 Parkfield earthquake, *J. Geophys. Res. Solid Earth*, 116 (B8).

530

531 Dieterich, J. H. (1979), Modeling of rock friction: 1. Experimental results and constitutive
532 equations, *J. Geophys. Res.*, 84, 2161–2168.

533

534 Duputel, Z., Vergne, J., Rivera, L., Wittlinger, G., Farra, V., Hetényi, G., 2016. The 2015
535 Gorkha earthquake: a large event illuminating the Main Himalayan Thrust fault. *Geophys. Res.*
536 *Lett.* 43 (2517–2525), 2016G. <http://dx.doi.org/10.1002/L068083>.

537

538 Elliott, J., Jolivet, R., Gonzalez, P., Avouac, J.P., Hollingsworth, J., Searle, M.P., Stevens,
539 V.L., 2016. Himalayan megathrust geometry and relation to topography revealed by the Gorkha
540 earthquake. *Nature Geosci.* <http://dx.doi.org/10.1038/NGEO2623>.

541

Commenté [p30]: Absent du texte

542 Fan, W., Shearer, P.M., 2015. Detailed rupture imaging of the 25 April 2015 Nepal earthquake
543 using teleseismic P waves. *Geophysical Research Letters* doi:10.1002/2015GL064587

544
545 Fu, Y., Freymueller, J.T., 2012. Seasonal and long-term vertical deformation in the Nepal
546 Himalaya constrained by GPS and GRACE measurements. *J. Geophys. Res.* 117, B03407.
547 <http://dx.doi.org/10.1029/2011JB008925>.

548
549 Galetzka, J., Avouac, J.-P., Genrich, J.F., Hudnut, K.W., 2015. Slip pulse and resonance of
550 Kathmandu basin during the 2015 Mw 7.8 Gorkha earthquake, Nepal imaged with geodesy.
551 *Science*, ISSN 0036-8075.

Commenté [p31]: Absent du texte

552
553 Grandin, R., Vallée, M., Satriano, C., Lacassin, R., Klinger, Y., Simoes, M., Bollinger, L., 2015.
554 Rupture process of the Mw = 7.9 2015 Gorkha earthquake
555 (Nepal):<http://dx.doi.org/10.1016/j.jseae.2016.05.028> insights into Himalayan megathrust
556 segmentation. *Geophys. Res. Lett.* 42 (20), 8373–8382.

557
558 Gualandi, A., Avouac, J. P., Galetzka, J., Genrich, J. F., Blewitt, G., Adhikari, L. B., & Liu-
559 Zeng, J., 2016. Pre-and postseismic deformation related to the 2015, Mw7. 8 Gorkha
560 earthquake, Nepal. *Tectonophysics*, DOI: 10.1016/j.tecto.2016.06.014.

561
562 Hubbard, J., Almeida, R., Foster, A., Sapkota, S. N., Bürgi, P., & Tapponnier, P., 2016.
563 Structural segmentation controlled the 2015 Mw 7.8 Gorkha earthquake rupture in Nepal.
564 *Geology*, 44(8), 639-642.

565
566 Hugentobler U., Schaer S., Fridez, P., Bernese GPS Software Version 4.2, Astronomical
567 Institute, University of Berne, Switzerland, 2001.

568
569 Jouanne, F., Mugnier, J.L., Pandey, M., Gamond, J.F., Le Fort, P., Serrurier, L., Vigny, C.,
570 Avouac, J.-P., 1999. Oblique convergence in the Himalayas of western Nepal deduced from
571 preliminary results of GPS measurements. *Geophys. Res. Lett.* 26 (13), 1933–1936.

Commenté [p32]: Absent du texte

572
573 Jouanne, F., Mugnier, J.L., Gamond, J.F., Le Fort, P., Pandey, M., Bollinger, L., Flouzat, M.,
574 Avouac, J.P., 2004. Current shortening across the Himalayas of Nepal. *Geophys. J. Int.* ,157,
575 1–14.

576
577 Jouanne, F., A. Awan, A. Madji, A. Pêcher, M. Latif, A. Kausar, J. L. Mugnier, I. Khan, and N.
578 A. Khan, 2011. Postseismic deformation in Pakistan after the 8 October 2005 earthquake:
579 Evidence of afterslip along a flat north of the Balakot-Bagh Thrust, *J. Geophys. Res.*, **116**,
580 B07401, doi:[10.1029/2010JB007903](https://doi.org/10.1029/2010JB007903).

581
582 Jouanne F, Awan A, Pêcher A, Kausar A, Mugnier JL, Khan I, NA Khan, Van Melle J., 2014.
583 Present-day deformation of northern Pakistan from Salt Ranges to Karakorum Ranges, *J.*
584 *Geophys. Res. Solid Earth*, 119 (3), 2487-2503.

585
586 Jouanne F., Mugnier J.L., Sapkota S. N., Bascou B., Pecher A., 2017. Estimation of coupling
587 along the Main Himalayan Thrust in the central Himalaya, *Journal of Asian earth sciences*,
588 January 2017.

589
590 Kayal, J.R., 2008. Microearthquake Seismology and Seismotectonics of South Asia.
591 <http://dx.doi.org/10.1007/978-1-4020-8180-4>.

592
593 Kulhawy, F.H. (1975). Stress deformation properties of rock and rock
594 discontinuities. *Engineering Geology*, Vol. 9, pp 327-350.

595 Kumar A., Singh SK, Mitra S, Priestley K.F., Shankar Dayal , 2017. The 2015 April 25 Gorkha
596 (Nepal) earthquake and its aftershocks: implications for lateral heterogeneity on the Main
597 Himalayan Thrust, *Geophys. J. Int.*, 208 (2): 992-1008.

598
599 Hutton, W., DeMets, C., Sánchez ,O., Suárez, G., Stock, J., 2001. Slip dynamics during and
600 after the 9 October 1995 Mw = 8.0 Colima-Jalisco, Mexico, *Geophys. J. Int.*, 146, 637–658,
601 doi:10.1046/j.1365- 246X.2001.00472.x.

602
603 Lindsey, E.O., Natsuaki, R., Xu, X., Shimada, M., Hashimoto, M., Melgar, D., Sandwell, D.T.,
604 2015. Line-of-sight displacement from ALOS-2 interferometry: Mw 7.8 Gorkha Earthquake
605 and Mw 7.3 aftershock. *Geophysical Research Letters* 42, 6655–6661.
606 doi:10.1002/2015GL065385.

607

Commenté [p33]: Absent du texte

608 Melbourne, W.G., 1985. The case for ranging in GPS based geodetic system. Paper Presented
609 at 1st International Symposium on Precise Positioning with the Global Positioning System, Int.
610 Assoc. of Geod., Rockville, Md.

Commenté [p34]: déplacé

611

612 Melnick, D, Moreno, M., Cisternas, M., Tassara, A , 2012. Darwin seismic gap closed by the
613 2010 Maule earthquake. *Andean Geology*, v. 39, no. 3, p. 558-563.

614

615 Mencin, D., Bendick, R., Upreti, B. N., Adhikari, D. P. Gajurel, A. P., Bhattarai, R. R.,
616 Shrestha, H. R., Bhattarai, T. N., Manandhar, N., Galetzka, J., Knappe, E., Pratt-Sitaula, B.,
617 Aoudia A. & Bilham R., 2016. Himalayan strain reservoir inferred from limited afterslip
618 following the Gorkha earthquake. *Nature Geoscience* , 9, 533–537. doi:10.1038/ngeo2734

619

620 Moreno, M., Melnick, D., Rosenau, M., Baez, J., Klotz, J., Oncken, O., Tassara, A., Chen, J.,
621 Bataille, K., Bevis, M., Socquet, A., Bolte, J., Vigny, C., Brooks, B., Ryder, I., Grund, V.
622 Smalley, B., Carrizo, D., Bartsch, M., Hase, H. , 2012, Toward understanding tectonic control
623 on the M w 8.8 2010 Maule Chile earthquake. *Earth and Planetary Science Letters*, v. 321-322,
624 p. 152-165.

625

626 Mugnier, J.L., Huyghe, P., Leturmy, P., Jouanne, F., 2004. Episodicity rates of thrust sheet
627 motion in the Himalayas (western Nepal). In: *McClay, K. (Ed.), Thrust Tectonics and*
628 *Hydrocarbon Systems, vol. 82. A.A.P.G. Memoir*, pp. 91–114.

Commenté [p35]: absent du texte

629

630 Mugnier, J.L., Huyghe, P., Gajurel, A., Upreti, B.N., Jouanne, F., 2011. Seismites in the
631 Kathmandu valley and seismic hazard in central Himalaya. *Tectonophysics*.
632 <http://dx.doi.org/10.1016/j.tecto.2011.05.012>.

633

634 Mugnier, J.L., Gajurel, A., Huyghe, P., Jouanne, F., Upreti, B.N., 2013. Structural interpretation
635 of the great earthquakes of the last millennium in Central Himalaya. *Earth Sci. Rev.* 127, 30–
636 47. <http://dx.doi.org/10.1016/j.earscirev.2013.09.003>.

637

638 Mugnier J.-L., Jouanne F., Bhattarai R., Cortes-Aranda J., Gajurel A., Leturmy P., Robert X.,
639 Upreti B., Vassallo R. , 2017. Segmentation of the Himalayan megathrust around the Gorkha
640 earthquake (25 April 2015) in Nepal. *Journal of Asian Earth Sciences*.

641

642 Nelson K. and 26 others., 1996. Partially Molten Middle Crust Beneath Southern Tibet:
643 Synthesis of Project INDEPTH Results. *Science*, 274, 1684-1687
644

645 Oldham, T., 1883. A catalogue of Indian earthquakes from the earliest time to the end of 1869
646 AD. *Mem. Geol. Survey India* 1, 163–215.
647

648 Ostini, L., Dach, R., Meindl, M., Schaer, S., Hugentobler, U., 2008. FODITS: a new tool of the
649 Bernese GPS software. In: Torres, J.A., Hornik, H. (Eds.), *Proceedings of EUREF 2008*
650 *Symposium*, Brussels, Belgium.
651

652 Perfettini, H., Avouac, J. - P., 2004. Postseismic relaxation driven by brittle creep: A possible
653 mechanism to reconcile geodetic measurements and the decay rate of aftershocks, application
654 to the Chi-Chi earthquake, Taiwan, *J. Geophys. Res.*, 109, B02304,
655 doi:10.1029/2003JB002488.
656

657 Robert, X., Van Der Beek, P., Braun, J., Perry, C., Mugnier, J.L., 2011. Control of
658 detachment geometry on lateral variations in exhumation rates in the Himalaya: Insights from
659 low-temperature thermochronology and numerical modeling. *Journal Geophysical Research*
660 *Solid Earth* 116, 1–22. doi:10.1029/2010JB007893
661

662 Rousset, B., Barbot, S., Avouac J.P0, Hsu, Y.J., 2012. Postseismic deformation following the
663 1999 Chi-Chi earthquake, Taiwan: Implication for lower-crust rheology, *J. Geophys. Res: Solid*
664 *Earth*, 117 (B12).
665

666 Ruina, A. L. (1983), Slip instability and state variable friction laws, *J. Geophys. Res.*, 88,
667 10,359–10,370.
668

669 Scholz, C.H., 1998. Earthquakes and friction laws. *Nature* 391, 37– 42.
670

671 Szeliga, W., Hough, S., Martin, S., Bilham, R., 2010. Intensity, magnitude, location, and
672 attenuation in India for felt earthquakes since 1762. *Bull. Seismol. Soc. Am.* 100, 570–584.
673 <http://dx.doi.org/10.1785/0120080329>.
674

675 Wang, K., Fialko, Y., 2014. Space geodetic observations and models of postseismic
676 deformation due to the 2005 M7.6 Kashmir (Pakistan) earthquake, *J. Geophys. Res.*, 119, 7306-
677 7318.

678
679 Wübbena, G., 1985. Software developments for geodetic positioning with GPS using TI4100
680 code and carrier measurements. Paper Presented at 1st International Symposium on Precise
681 Positioning with the Global Positioning System, *Int. Assoc. of Geod.*, Rockville, Md.

682
683 Yu, S.-B., Y.-J. Hsu, L.-C. Kuo, H.-Y. Chen, and C.-C. Liu, 2003. GPS measurement of
684 postseismic deformation following the 1999 Chi-Chi, Taiwan, earthquake, *J. Geophys. Res.*,
685 108(B11), 2520, doi:10.1029/2003JB002396.

686
687 **Zhao, W., Nelson, K.D., Che, J., Quo, J., Lu, D., Wu, C., Liu, X., 1993. Deep seismic reflection**
688 **evidence for continental underthrusting beneath southern Tibet. *Nature*, 366, 555–559.**

Commenté [p36]: Absent du texte

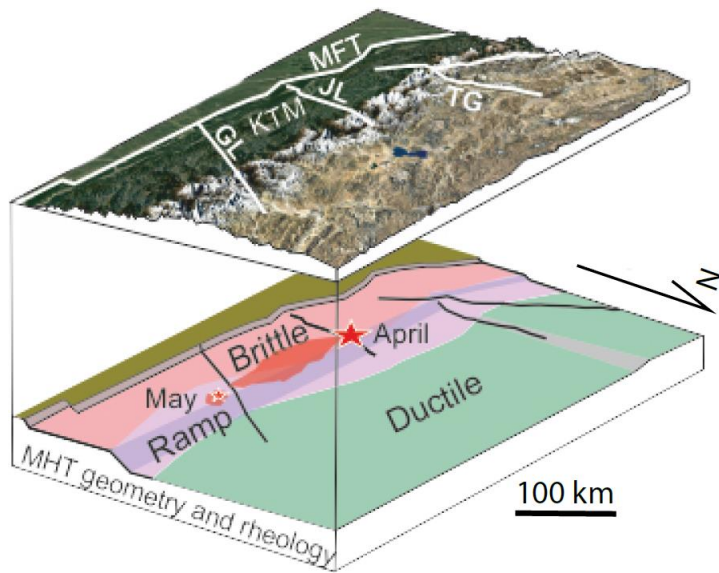
689
690
691
692
693
694
695
696
697
698
699
700
701
702
703
704
705
706
707
708

709
710
711
712
713
714
715
716
717
718
719
720

cGNSS Stations	Amplitude of the seasonal component in mm	Phase difference in days	cGNSS stations installed after the Gorkha earthquake	Interpolated amplitude values for the seasonal component in mm	Interpolated phase difference values in days
BESI	1.66	154.50	BALE	1.71	107.96
BRN2	0.95	98.29	BHAZ	1.96	70.64
CHLM	2.81	95.05	CHAR	1.56	115.30
DAMA	2.03	121.64	DNC4	2.37	78.93
GUMB	3.75	103.16	GUMB	1.88	98.56
KKN4	1.60	75.06	GURJ	1.62	74.39
KLDN	1.52	109.80	JIR2	1.50	115.64
LMJG	2.00	102.70	SLBL	1.70	119.67
NAST	1.96	120.66	TSM1	2.62	142.31
ODRE	1.60	107.24	XBAR	1.70	106.86
RMJT	1.14	93.10			
RMTE	0.76	139.44			
SNDL	1.42	127.03			
SYBC	1.42	130.12			
TPLJ	2.03	95.93			

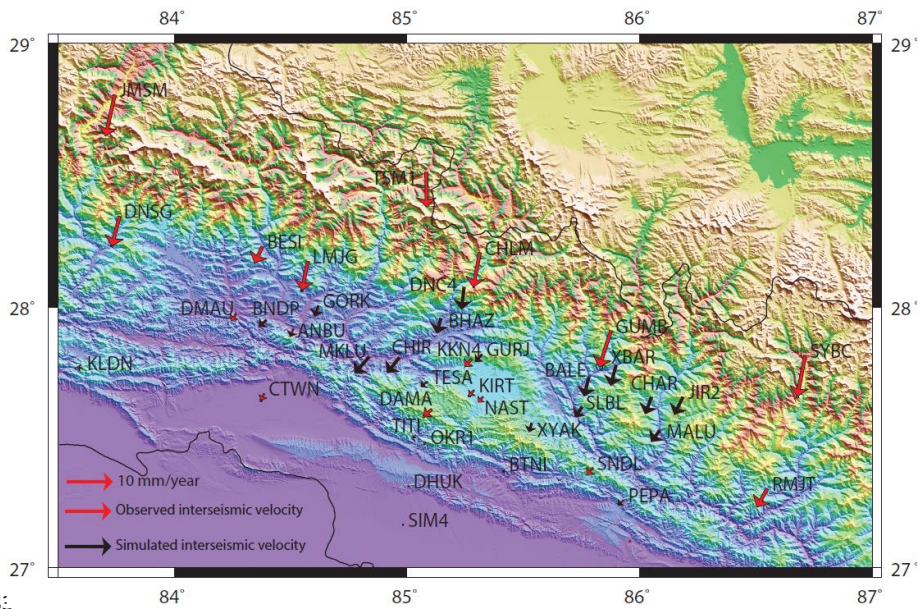
721
722
723
724
725
726

Table 1. Seasonal components affecting the south component of the time series. These values were estimated by FODITS, Bernese 5.2 software (Ostini et al., 2008) for the cGNSS stations that were installed several years before the Gorkha earthquake or interpolated using the values previously estimated for the stations installed after the Gorkha earthquake.



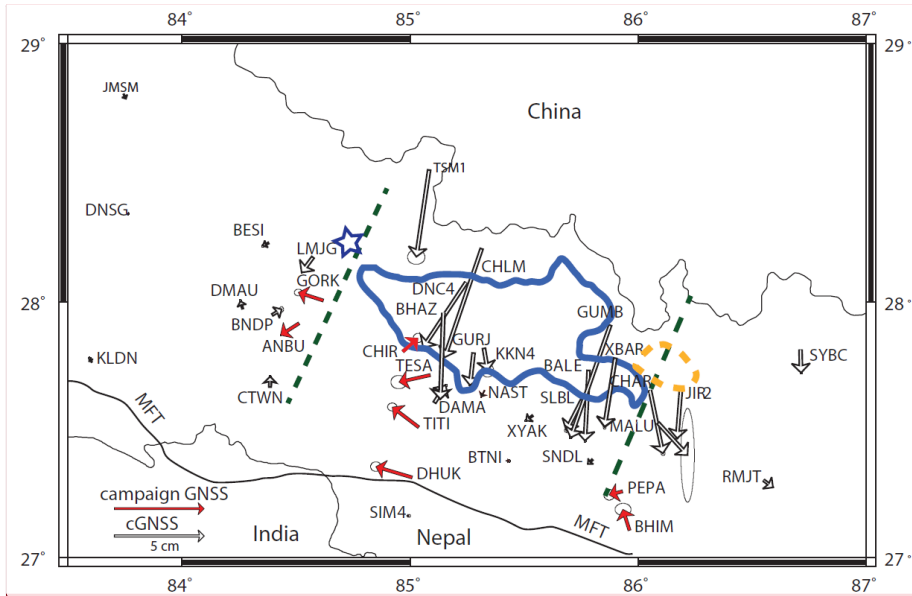
727
 728
 729
 730
 731
 732

Figure 1. Location of the Gorkha earthquake along the upper flat of the MHT. Heavy purple for ramp geometry; pink, light purple and green for fully locked, partial coupled and ductile MHT, respectively; red for rupture zones. The rupture area is bounded by lateral ramps



734 *Figure 2. Observed (Jouanne et al., 2017) and simulated interseismic velocities using*
 735 *the model proposed by Jouanne et al. (2017). Velocities are expressed in the India fixed*
 736 *reference frame.*

737
 738



739

740

741 *Figure 3. Postseismic displacements following the Gorkha earthquake for the June 24, 2015-*
 742 *December 2016 period. The recorded displacements are corrected for interseismic*
 743 *displacements.*

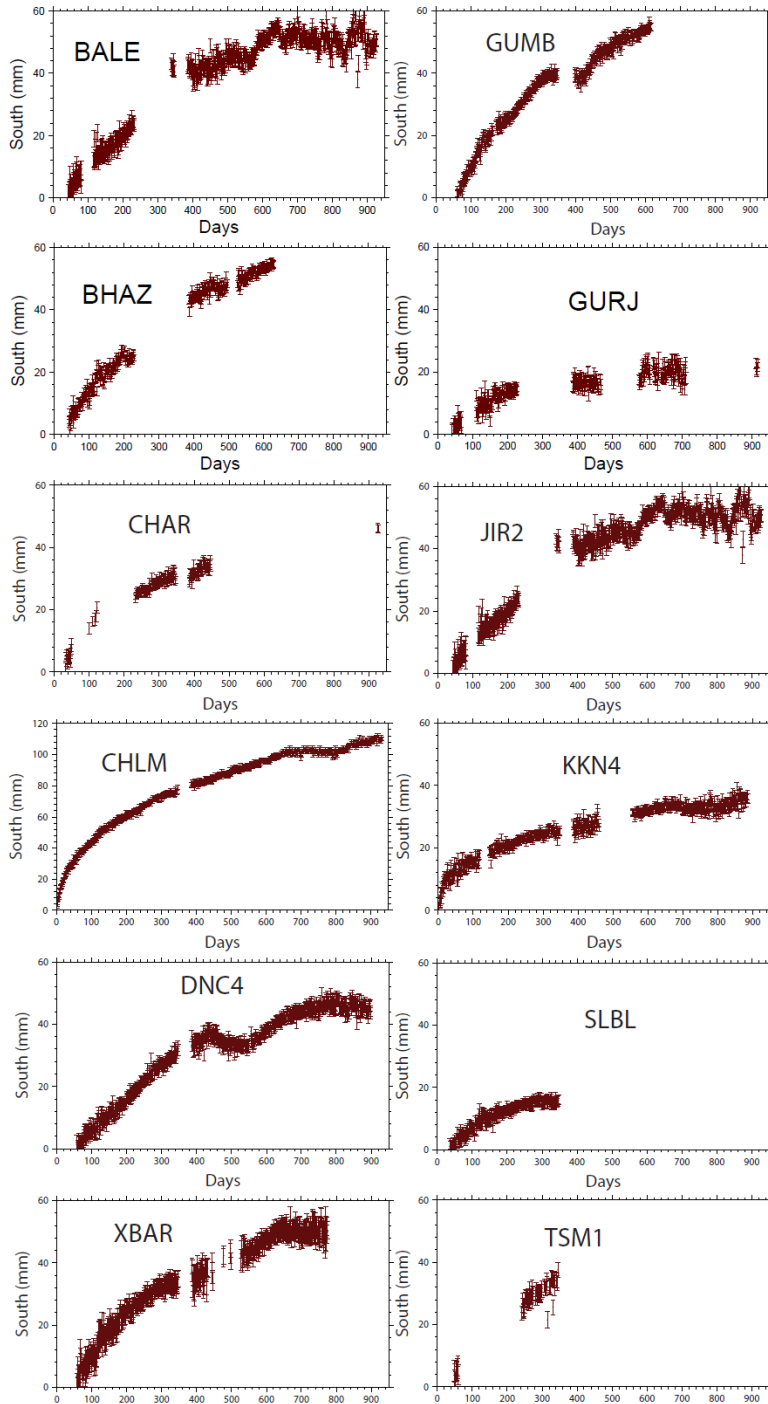
744 *The rupture of the Gorkha earthquake is indicated by a blue line and the rupture of its main*
 745 *aftershocks, on May 12, 2016, is drawn with an orange line. The star indicates the nucleation*
 746 *of the Gorkha earthquake to the west of its rupture. The dashed green lines indicate the location*
 747 *of the Judi lineament (Kaya, 2008) that separates the main rupture zone from the nucleation*
 748 *area (Kumar et al., 2017) and, on the eastern side, the Gaurishankar lineament (Mugnier et*
 749 *al., 2017). Errors ellipses are drawn for a 95% confidence level.*

750

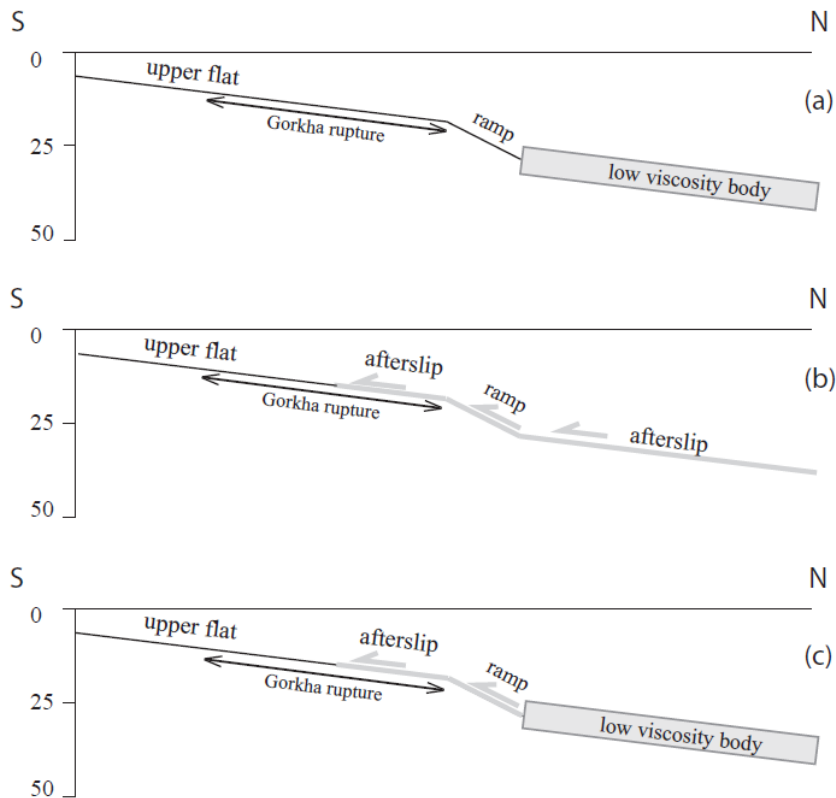
Commenté [M37]: La position des deux linéaments est assez piffométrique : regarde plutôt notre article de 2017 !

Commenté [M38]:

Commenté [M39]: Il faudrait mettre quelques lignes d'isovaleurs du glissement (et indiquer la valeur retenue pour les lignes jaunes et bleues)



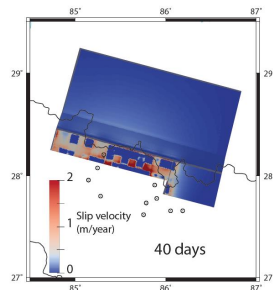
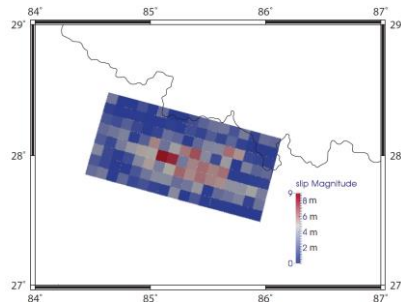
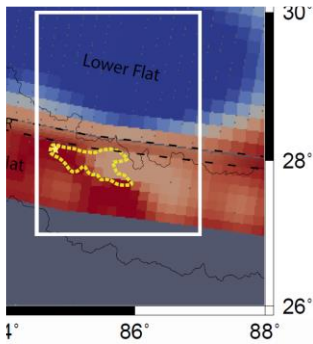
752 *Figure 4. South components for the cGNSS station displacements, corrected from interseismic*
 753 *velocities and seasonal signals estimated during the period before the main shock or*
 754 *extrapolated for the new stations. The locations of cGNSS stations are indicated on Figure 2.*
 755



756
 757 *Figure 5. Geometry and rheological properties considered in the numerical simulations*
 758 *of postseismic deformation. (a) Viscous relaxation controlled by a high fluidity body embedded*
 759 *in a half-space characterized by a low fluidity, (b) afterslip along the northern part of the upper*
 760 *flat of the MHT, along the ramp, and along the lower flat of the MHT and (c) viscous relaxation*
 761 *controlled by a high fluidity body embedded in a half-space characterized by a low fluidity and*
 762 *afterslip along the crustal ramp and along the northern part of the upper flat.*

763
 764
 765

Commenté [j140]: CETTE FIGURE EST PROCHE DE LA FIGURE 37B3 : LA SEULE DIFFERENCE, C'EST LES DEUX STATIONS NON MODÉLISÉES ET L'ABSENCE DES COURBES MODÉLISÉES : POURQUOI NE PAS FAIRE UNE SEULE FIGURE ? (ENFIN JE COMPRENS L'IDEE DE SÉPARER DONNÉES ET RÉSULTAT DU MODÈLE..°



766

767

768

769

770

771

772

773

774

775

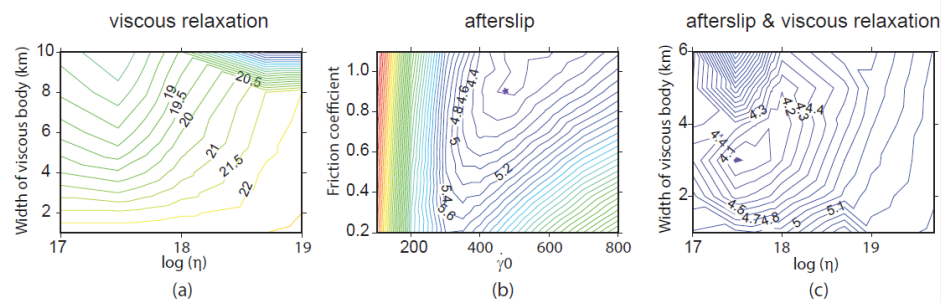
776

777

Figure 6. Description of the inter and co-seismic and post deformation on the 3 ? km mesh used for the modeling of the deformation with the Relax software. a) Coupling along the Main Himalayan Thrust during the interseismic period (before the Gorkha earthquake) (modified from Jouanne et al., 2017). The white rectangle indicates the location of Figure 9. CR indicates the location of the crustal ramp. b) Coseismic slip distribution (adapted from Grandin et al., 2016), and used as input for our numerical simulation. c) an example of the post-seismic deformation (PAR EXEMPLE TU DEVRAIS PRESENTER LE DEPLACEMENT POSTSEISMIQUE CUMULE POUR preferred afterslip model ET TU DEVRAIS PLACER SUR TOUTES CES FIGURES LE TRACE DE LA RUPTURE DE AVRIL et CELLE DE MAI

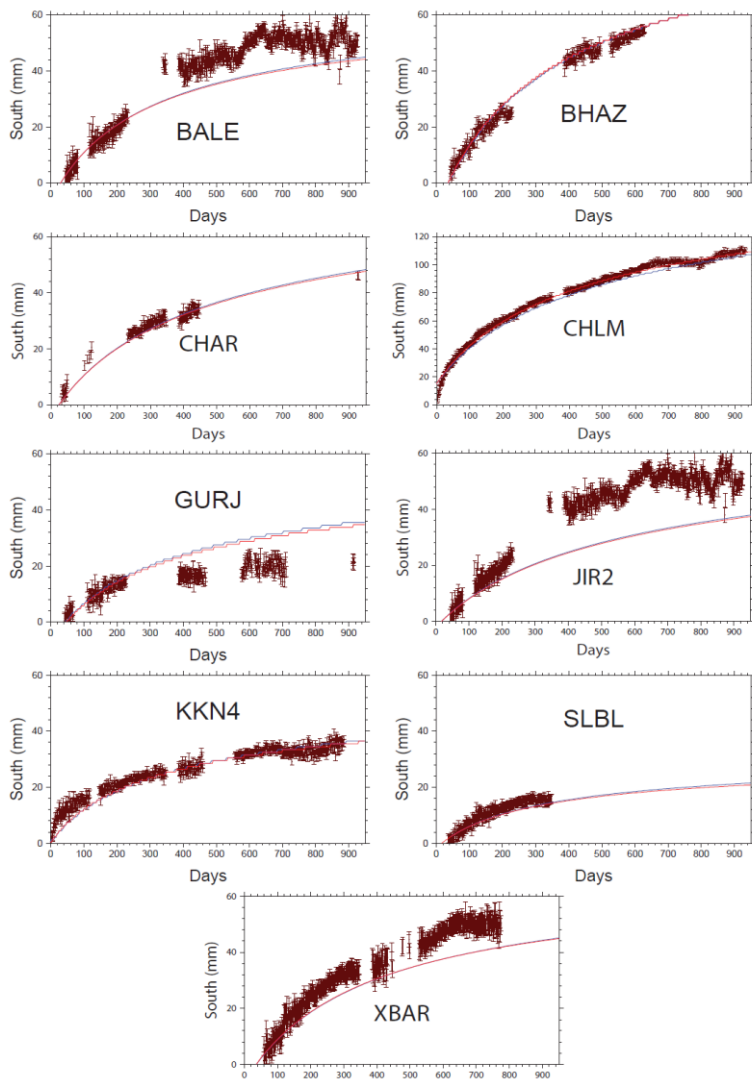
Commenté [j141]: Représenter la limite de la rupture par une ligne par dessus

Commenté [M42]: le décalage du maillage au front correspond tres bien avec la terminaison sud de la rupture de Mai! Ca permettra de visualizer tout cela



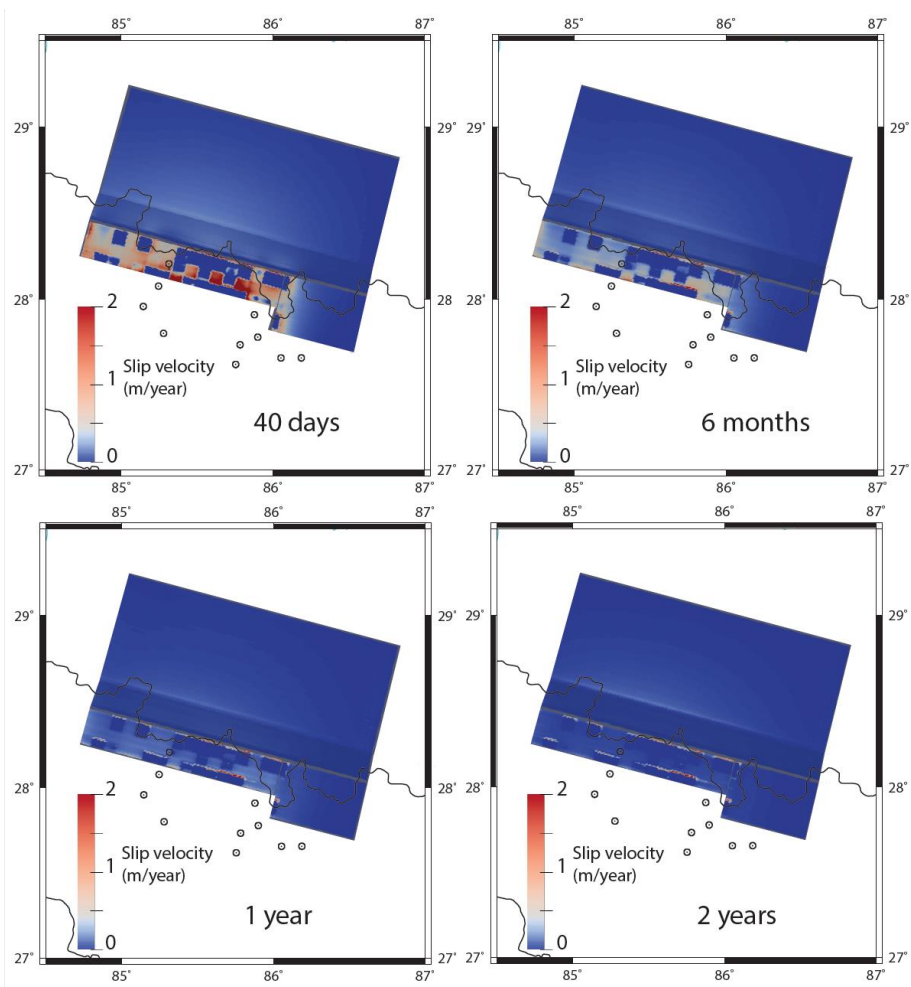
778

779 *Figure 7. Research of the best solution, with the plot of the WRMS, for (a) the viscous relaxation*
 780 *hypothesis controlled by a viscous body along the lower flat of the MHT, (b) afterslip hypothesis*
 781 *and (c) afterslip and viscous relaxation controlled by a viscous body along the lower flat of the*
 782 *MHT. The best solution for the afterslip hypothesis is indicated by a star, and by a polygon for*
 783 *the afterslip & viscous relaxation.*



784
 785 *Figure 8. Observed and simulated postseismic time series with our preferred afterslip model,*
 786 *the afterslip & viscous relaxation model and the viscous relaxation model. The simulated time*

787 series with our preferred afterslip and afterslip & viscous relaxation almost always become
 788 confused. Blue curve: afterslip hypothesis, red curve: afterslip and viscous relaxation
 789 controlled by a viscous body along the lower flat of the MHT. PROCHE DE LA FIGURE 4!
 790
 791
 792
 793



794
 795 Figure 9. Evolution over time and space of the slip velocity, predicted by our preferred afterslip
 796 model, expressed for select data from 0 +40 days to 0 +2 years, the velocity is expressed in

Commenté [M43]: Je sais pas si ton échelle de couleur est bien choisi : presque tout est bleu ???

Commenté [M44]: IL FAUDRAITINDIQUER SUR CETTE FIGURE OU SE SITUE LA RAMPE

Commenté [M45]: Les localisations des sites sont difficiles à voir !

Commenté [M46]: JE comprends pas ce que ça veut dire

797 *meters per year. The locations of the permanent GNSS stations used to constrain our modellings*
798 *are indicated by open circles.*
799
800